

# Evaluating the Performance of a Photofission Prompt Neutron Detection System Based on Threshold Activation Scintillation Coupled with a 9 MeV Electron Accelerator

Luna Sobczak<sup>1,\*</sup>, Adrien Sari<sup>1</sup>, and Frédéric Carrel<sup>1</sup>  
<sup>1</sup>Université Paris-Saclay, CEA, List, 91120 Palaiseau, France  
(\* ) [luna.sobczak@cea.fr](mailto:luna.sobczak@cea.fr)

**Abstract**—Developments in photofission prompt neutron detection are crucial in nuclear instrumentation, whether for waste characterization and security applications. *Bremsstrahlung* photons, emitted by a linear electron accelerator (linac), can induce photofission reactions when interacting with actinides. These reactions then emit prompt and delayed neutrons and delayed gammas. However, the intense photon flash from the linac saturates detection systems, commonly He-3 proportional counters, making prompt neutron instantaneous detection challenging. This study evaluates a photofission prompt neutron detection system coupled with a 9 MeV linac to investigate the use of prompt neutrons as a third signature, alongside delayed neutrons and gammas. This to reduce uncertainties in detecting, differentiate and quantify actinide despite an attenuated interrogating flux or absorbed photofission particles by the environment. First, with Monte Carlo codes PHITS and MCNP6 and their respective nuclear data libraries (ENDF/B-VIII.0 and JENDL-5), we assessed the parameter of a photofission setup which consists in detecting the delayed 6.131 MeV gamma radiation emitted by N-16 decay, resulting from (n,  $\alpha$ ) activation of F-19. This approach avoids the impact of the linac's photon flash and minimizes the strong photoneutron background. Secondly, we conducted experimental tests with neutron sources and then with a 9 MeV electron accelerator, Linatron® M9A (Varex Imaging Corp.), at the SAPHIR platform (CEA Paris-Saclay, France), using machined polytetrafluoroethylene and a bismuth germanate scintillator to detect prompt neutrons from a depleted UMo sample. This work enhances prompt neutron detection developments and contributes to advancements in characterizing special nuclear materials (SNMs) by photofission for various applications.

**Keywords**—Linear electron accelerator (linac), Active Photon Interrogation (API), photofission, prompt neutrons, threshold activation detector (TAD), fluorine.

## I. CONTEXT AND CHALLENGES

A photon with enough energy ( $> 6$  MeV) interacting with actinides, i.e., U-235, U-238, Pu isotopes, may generate a photofission reaction, emitting various particles at different

emission time. The emission of prompt neutrons and prompt gammas occurs simultaneously with the fission fragments and the delayed particle are emitted later by the fission product [1, 2]. The photon beam is usually induced by a linear electron accelerator (linac), that converts electrons into high-energy *Bremsstrahlung* photons, by slowing them on heavy atomic nuclei target such as tungsten or tantalum for instance. Photofission is a reaction of great interest for research and development in the field of nuclear instrumentation and more specifically in non-destructive active nuclear measurement technique such as active photon interrogation (API) method. The latter finds many applications in the fields of quantification of fissile material for nuclear/radioactive waste package characterization, and storage [3–15], for homeland security or border control [16–19], to counter proliferation, and for fundamental nuclear physics [20].

The API method addresses passive emission detection difficulties and, furthermore, overcomes common attenuation of interrogating neutron beams by using photons which have an enhanced penetrating capability. In this context, prompt photofission neutron detection is particularly relevant to counter matrix effects in radioactive waste packages or shielding of SNM in cargo containers. That is to say, when measurements are complicated by self-absorption and the attenuation of photofission particles like gamma signatures and mainly delayed neutrons thermalization in hydrogenated materials. In spite of this, most applications regarding photofission particles emission concerns delayed neutrons and delayed gammas. This, because prompt neutrons are emitted instantaneously while the measurement system and electronics, commonly He-3 proportional counters, are saturated by the intense photon flash delivered by the linac and under a strong photoneutron background created in the conversion target and surrounding materials [21].

An indirect detection method based on threshold activation detectors (TAD) has been deployed since the earliest advancements in neutron detection for nuclear reactors and then applied to prompt neutron detection [22,23]. More recent progress has been led by developments with pentafluorostyrene plastic scintillator and CaF<sub>2</sub> TAD in nuclear waste package and

homeland security applications [24–26]. It consists in delaying the measurement of prompt neutrons by detecting the delayed 6.131 MeV gamma radiation emitted by N-16 decay, resulting from  $(n, \alpha)$  activation of F-19. These detectors enable firstly to bypass the gamma blinding by delaying the detection in time and secondly to avoid the background noise of photoneutrons produced in the tungsten target, collimator and surrounding materials during the photon beam production.

In this paper, we firstly present the photofission prompt neutron detection setup geometry designed based on the TAD indirect method and the Monte Carlo simulations we performed to assess its parameters. In a previous study, we evaluate with MCNP6 [27, 28] the photoneutron background produced in the tungsten of the accelerator considering the  $(\gamma, n)$ ,  $(\gamma, 2n)$  and  $(\gamma, Xn)$  cross-sections and reaction threshold, also the photofission reaction rate in a uranium sample. Here, after reviewing these key quantities, we evaluate the  $(n, \alpha)$  reaction rate on PTFE induced by the prompt neutron and photoneutron yield mentioned. Secondly, we report the results of two experimental campaigns conducted using machined polytetrafluoroethylene layers placed against a bismuth germanate scintillator. The first campaign involved tests with characterized AmBe and Cf-252 neutron sources from the LNHB (Laboratoire National Henri Becquerel). The second campaign utilized the 9 MeV linac of the SAPHIR platform at CEA Paris-Saclay to irradiate a depleted UMo sample.

## II. DESIGN OF A DETECTION SYSTEM BY SIMULATION

To design the mentioned system, we modeled and simulated the following geometry with MCNP6 and PHITS [29, 30] Monte Carlo codes. The setup in Fig. 1 includes the accelerating portion of the linac in green, to wit, the pipe where the electron beam is accelerated. In addition, the conversion target on its copper stand, holding the *Bremsstrahlung* reactions and the collimator are both made of heavy nuclei, here tungsten. The sample is a depleted 7.5 cm-high uranium cylinder with a radius of 0.7 cm. The detector section is composed of a 7.62 cm  $\times$  7.62 cm bismuth germanate scintillator crystal ( $\text{Bi}_4\text{Ge}_3\text{O}_{12}$ ), wrapped up with a fluoropolymer layer of polytetrafluoroethylene (PTFE,  $\text{C}_2\text{F}_4$ ), known as Teflon®. The latter operates as the activated fluoride converter.

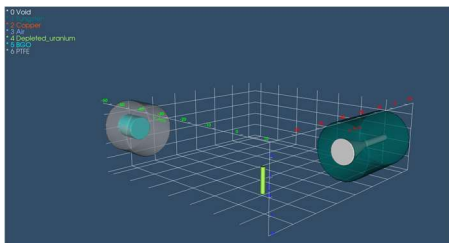


Fig. 1. MCNP6 photofission model visualization with 3D PHITS visualizer PHIG-3D

In a previous study we characterized the photofission rate and the corresponding background noise produced by a linac operating at 6, 9, 15 or 18 MeV. Given the 7 MeV energy threshold of the  $(\gamma, n)$  reaction on tungsten, the  $(\gamma, 2n)$  reactions

involved for processes beyond 10 MeV, and the 6 MeV photofission barrier, prompt neutron detection frame was concluded more efficient with an operating energy of 9 MeV. Indeed, the photoneutron yield happens to be 90 times higher for a linac operated at 15 MeV compared to 9 MeV. Then calculation of the photofission reaction rate in a uranium sample leads to the conclusion that the signal-to-noise ratio is optimal for an accelerator operated at 9 MeV, i.e., for a photoneutron production about 24 times higher than the prompt neutron yield. In Table I, we registered different evaluated yield rates: both the prompt neutron yield with  $(\gamma, f)$  photofission reaction rate in uranium, the photoneutron yield with the  $(\gamma, Xn)$  photoneuclear reaction rate in tungsten target and collimator, and also the related signal to noise ratio.

Table I SIGNAL-TO-NOISE RATIO EVALUATION FOR A LINAC OPERATING AT 9 MEV

Electron energy (MeV)	$(\gamma, f)$ (n.s <sup>-1</sup> )	$(\gamma, Xn)$ (n.s <sup>-1</sup> )	$(\gamma, f)/(\gamma, Xn)$ ratio
9	$1.24 \times 10^{11}$	$2.94 \times 10^{12}$	$4.24 \times 10^{-2}$

Results obtained using the MCNP6 Monte Carlo code. A previous study employed also the PHITS code and both were run with their respective library (ENDF/B-VIII.0 and JENDL-5) and with the library of the other code to intercompare the impacts on the results.

The previous reaction rates indicate the prompt neutron ( $n_p$ ) and photoneutron ( $n_\gamma$ ) production per second and this gives the different neutron contributions in PTFE activation by  $(n, \alpha)$  reactions. Given in Table II, the  $(n, \alpha)$  reaction rate on PTFE induced by the two aforementioned neutron sources and the related ratio.

Table II PTFE ACTIVATION BY  $(n, \alpha)$  REACTION

Electron energy (MeV)	$(n_p, \alpha)$ (reac.s <sup>-1</sup> )	$(n_\gamma, \alpha)$ (reac.s <sup>-1</sup> )	$(n_p, \alpha)/(n_\gamma, \alpha)$ ratio
9	$4.57 \times 10^6$	$1.26 \times 10^4$	$3.63 \times 10^2$

Finally, a study on thickness optimization was conducted alongside the calculation of the signal-to-noise ratio given by the prompt neutron and photoneutron production, and the assessment of their contribution in the  $(n, \alpha)$  reaction rate. This combined analysis led to the following conclusion regarding how the betas and gammas lose their energy in the materials:

→ 5 cm of PTFE ( $2.25 \text{ g.cm}^{-3}$ ) stops 25% of 6 MeV gammas and all beta particles.

→ 10 MeV  $\beta$  will deposit all its energy in 0.85 cm of BGO and 2.6 cm of PTFE.

From this, we conclude that we will be able to detect gamma particles but only the beta produced near the BGO in the very first centimetres of PTFE surrounding the crystal.

The evaluation of the reaction products' propagation led to efficiency and sensitivity calculation. The detection efficiency of the BGO is simulated with MCNP6 F8 tally, for the detection of beta and gamma particles produced in PTFE. In a first place,

we assumed a homogeneous 6.1 MeV gamma source uniformly distributed within the PTFE volume and same procedure for beta particles with  $^{19}\text{F}$  decay beta spectrum. We obtain the following efficiencies:

- 5.17% for 6.1 MeV gamma
- 0.68% for  $\beta$  spectrum of  $^{19}\text{F}$  decay

The expected sensitivities are calculated for the following experimental configuration: a linac operated at 9 MeV and pulse frequency of 100 Hz, a 240 g depleted uranium sample, and an acquisition of 60 s after 60 s of irradiation. Given that the half-life of N-16 is 7.13 s, the equilibrium production–decay is achieved within approximately 36 s. Therefore, we optimize the N-16 production in PTFE and with a 60 s acquisition we nearly measure the full signal.

We obtain the following sensitivities, illustrating a favorable configuration for optimizing the signal-to-noise ratio:

- $(1.01 \pm 0.01) \times 10^{-1} \text{ c.s}^{-1}$  due to prompt neutrons
- $(2.80 \pm 0.04) \times 10^{-4} \text{ c.s}^{-1}$  due to photoneutrons

### III. EVALUATION OF THE PERFORMANCE IN LABORATORY CONDITIONS

Ahead of the irradiation campaign at the SAPHIR platform, we moved the photofission prompt neutron detection system to be irradiated under laboratory conditions, that is to say, with metrologically characterized AmBe and Cf-252 neutron sources from the LNHB. This campaign allows to quantify and validate the discrepancy in the  $(n, \alpha)$  reaction rate in Teflon as a function of the energy spectrum of the sources, whose uncertainty on the emission rates are very low. It also allows us to obtain an experimental reference value for the  $(n, \alpha)$  reaction rate for a Cf-252 spectrum which is close to the prompt neutron spectrum.

The joint objective of the two following experiments is to activate with a neutron source the fluorine contained in a Teflon layer and identify the decay products from the reaction  $^{19}\text{F}(n, \alpha)^{16}\text{N}$  with a scintillator. The experimental parameters of the setup in Fig. 2 consist in an AmBe or Cf-252 neutron source with a  $9.51 \times 10^5 \text{ n.s}^{-1}$  and  $5.411 \times 10^6 \text{ n.s}^{-1}$  neutron emission rate respectively, known to within less than two percent uncertainty, irradiating a 5 cm hollow cylindrical PTFE converter in which a  $7.62 \text{ cm} \times 7.62 \text{ cm}$  BGO scintillator is placed. The detector is powered by a +800 V high voltage supplied by a CAEN DT1470ET module and the data is acquired with a Dspec502 spectrometer from Ortec. The protocol is a simultaneous irradiation and acquisition of 2700 s after the energy calibration with the following gamma emitting sources: Co-60, Y-88, Na-22, AmBe.

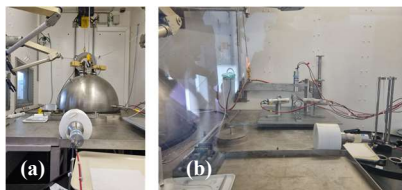


Fig. 2. (a) Back and (b) side view of the experimental setup at the LNHB casemate including the Cf-252 source and the BGO wrapped with the Teflon layer.

#### A. Irradiation with an AmBe neutron source

The gamma spectrum in Fig. 3 results from the activation of the PTFE layer by the AmBe neutron source ( $9.51 \times 10^5 \text{ n.s}^{-1}$ ) and includes the gamma emissions of the source itself, which has a photopeak at around 4.4 MeV. The high neutron energy spectrum of AmBe sources (around 4 MeV average energy) allowed us to identify the 6.131 MeV gamma product from the  $^{19}\text{F}(n, \alpha)^{16}\text{N}$  reaction as the cross section reaches 0.1 mb for 2.5 MeV incident neutrons.

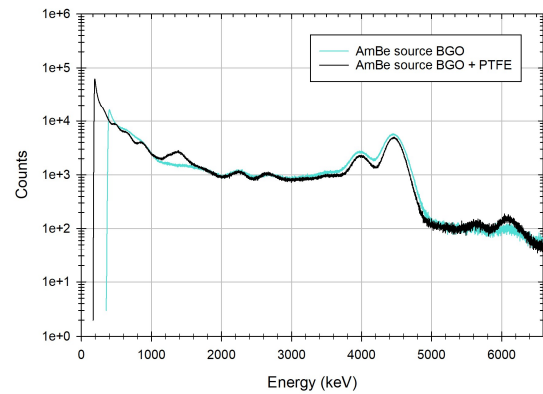


Fig. 3. Gamma spectra acquired after a 2700 s irradiation with an AmBe neutron source of a BGO scintillator (in blue) and a BGO wrapped in PTFE (in black).

Between 5.1 MeV and 7 MeV, the experimental peak net count rate obtained is of  $11.06 \pm 0.18 \text{ c.s}^{-1}$ . Also, complementary simulations of  $(n, \alpha)$  reaction rate on PTFE induced by the same AmBe neutron source will be modeled with MCNP6 to determine the  $(n, \alpha)$  reaction rate and the corresponding sensitivity.

#### B. Irradiation with a Cf-252 neutron source

The gamma spectrum in Fig. 4 results from the activation of the PTFE layer by the Cf-252 neutron source ( $5.411 \times 10^6 \text{ n.s}^{-1}$ ). The energy spectrum of Cf-252 neutron source is close to a Watt fission spectrum, with an average energy of about 2.1 MeV.

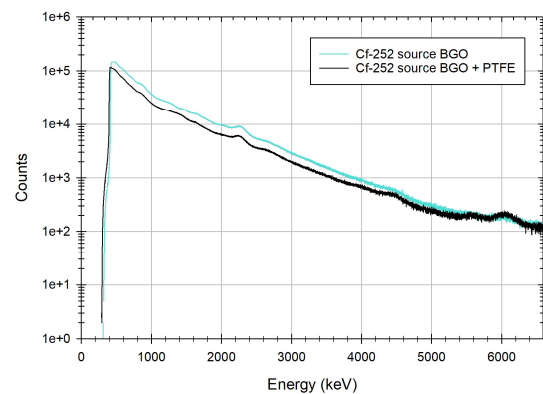


Fig. 4. Gamma spectra acquired after a 2700 s irradiation with a Cf-252 neutron source of a BGO scintillator (in blue) and a BGO wrapped in PTFE (in black).

Once more, the neutron contribution on the gamma spectrum is calculated between 5.1 MeV and 7 MeV and the experimental peak net count rate obtained is  $7.52 \pm 0.21 \text{ c.s}^{-1}$ . Complementary simulations of  $(n, \alpha)$  reaction rate on PTFE induced by the Cf-252 neutron source will be modeled with MCNP6 to determine the  $(n, \alpha)$  reaction rate and the corresponding sensitivity.

It should be noted that higher activation is observed with the AmBe source despite the Cf-252 source having a neutron emission rate nearly 6 times higher. This was expected and can be explained by the AmBe's harder energy spectrum.

#### IV. VALIDATION AT THE SAPHIR PLATFORM

Finally, we transferred the detection system at the SAPHIR platform. The source term is now a *Bremsstrahlung* photon beam produced by a linac operated at 9 MeV which irradiates the depleted uranium sample described earlier. All the other experimental parameters remain equivalent to the previous campaign at LNHB. The objective is to detect the decay product of the fluorine activation by the different neutron contributions and mainly the prompt neutrons from the photofission reactions in the sample. The protocol here consists in 60 s of acquisitions after 60 s of irradiation, following the energy calibration of the detector with Co-60, Cs-137 and AmBe gamma emitting sources.

With this method, we effectively highlight the signature of N-16. This demonstrates the feasibility of the detection system for a configuration based on a linac irradiation. The gamma spectrum in Fig. 5a shows an experimental peak net count rate of  $2.94 \pm 0.75 \text{ c.s}^{-1}$  in the 5.1 MeV and 7 MeV region of interest. The agreement between experimental and simulation results requires further investigation, particularly to characterize the systematic errors in the experiment. In Fig. 5b, the spectrum is obtained after placing a lead shield between the uranium sample and the PTFE cylinder. This added layer is decreasing the background noise around our ROI, thereby changing the experimental net peak area to total area ratio in our ROI from 0.03% to 0.19% by stopping the high-energy delayed gammas emitted by the sample. This result demonstrates that further improvements and optimizations remain possible.

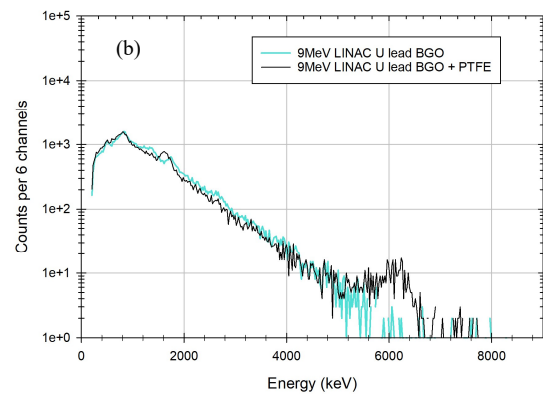
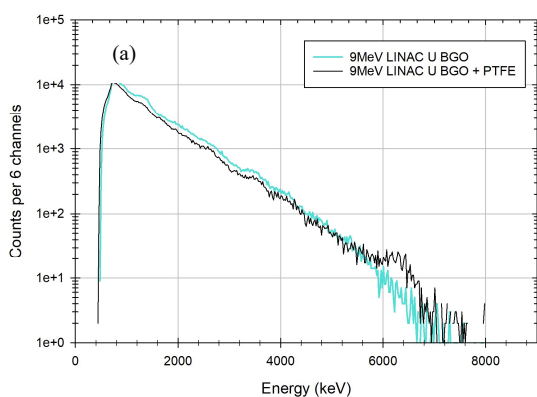


Fig. 5. Gamma spectrum acquired with (a) a BGO scintillator shielded with lead and (b) a BGO scintillator wrapped with PTFE and shielded with lead, after 60 s of irradiation and 60 s of acquisition with a 9 MeV linac.

#### V. CONCLUSIONS AND FUTURE DEVELOPMENTS

A photofission prompt neutron detection system was designed based on threshold activation detectors. After optimization through Monte Carlo simulations of the signal-to-noise ratio in a given configuration to enhance the detection sensitivity, we conduct several tests in laboratory conditions at the LNHB to validate the reliability of the system. Finally, we perform experiments at the SAPHIR platform using a 9 MeV linac to irradiate a uranium sample, produce photofission reactions and detect the gammas resulting from the fluorine activation from the prompt photofission neutrons.

Future work will include complementary acquisitions to characterize the signal resulting from the decay gamma emissions of N-16. Efforts will be made to optimize the reduction of photoneutron noise and improve the discrimination between prompt neutron contributions and high-energy delayed gammas. Simultaneous detection of delayed neutrons and prompt neutrons coupled with preliminary tests of inter-pulse acquisitions will also be performed.

#### REFERENCES

- [1] N. Bohr and J. A. Wheeler, "The Mechanism of Nuclear Fission," *Phys. Rev.*, vol. 56, no. 5, pp. 426–450, Sep. 1939, DOI: [10.1103/PhysRev.56.426](https://doi.org/10.1103/PhysRev.56.426).
- [2] R. O. Haxby, W.E. Shoupp, W. E. Stephens, and W.H. Wells, "Photofission of Uranium and Thorium," *Phys. Rev.*, vol. 58, no. 1, p. 92, Jul. 1940, DOI: [10.1103/PhysRev.58.92](https://doi.org/10.1103/PhysRev.58.92).
- [3] A. Lyoussi, J. Romeyer-Dherbey, F. Jallu, E. Payan, A. Buisson, G. Nurdin, *et al.*, "Transuranic waste detection by photon interrogation and on-line delayed neutron counting," *Nuclear Instrum. and Methods in Phys. Res. B*, vol. 160, no. 2, pp. 280–289, Feb. 2000, DOI: [10.1016/S0168-583X\(99\)00586-8](https://doi.org/10.1016/S0168-583X(99)00586-8).
- [4] M. Gmar, J. Jeanneau, F. Lainé, H. Makil, B. Poumarède, and F. Tolat, "Assessment of actinide mass embedded in large concrete waste packages by photon interrogation and photofission," *Appl. Radiat. Isot.*, vol. 63, no. 5–6, pp. 613–619, Dec. 2005, DOI: [10.1016/j.apradiso.2005.05.010](https://doi.org/10.1016/j.apradiso.2005.05.010).
- [5] F. Carrel, M. Agelou, M. Gmar, F. Lainé, B. Poumarède, and B. Rattoni, "Measurement of Plutonium in Large Concrete Radioactive Waste Packages by Photon Activation Analysis," *IEEE Trans. Nucl. Sci.*, vol. 57, no. 6, pp. 3687–3693, Dec. 2010, DOI: [10.1109/TNS.2010.2087356](https://doi.org/10.1109/TNS.2010.2087356).
- [6] F. Carrel, M. Agelou, M. Gmar, and F. Lainé, "Detection of high-energy delayed gammas for nuclear waste packages characterization," *Nuclear Instrum. and Methods in Phys. Res. A*, vol. 652, no. 1, pp. 137–139, Oct. 2011, DOI: [10.1016/j.nima.2010.08.014](https://doi.org/10.1016/j.nima.2010.08.014).

- [7] A. Sari, F. Carrel, F. Lainé, and A. Lyoussi, “Neutron interrogation of actinides with a 17 MeV electron accelerator and first results from photon and neutron interrogation non-simultaneous measurements combination,” *Nuclear Instrum. and Methods in Phys. Res. B*, vol. 312, pp. 30–35, Oct. 2013, DOI. [10.1016/j.nimb.2013.06.020](https://doi.org/10.1016/j.nimb.2013.06.020).
- [8] F. Carrel, B. Charbonnier, R. Coulon, F. Lainé, S. Normand, and C. Salmon, “Characterization of Old Nuclear Waste Packages Coupling Photon Activation Analysis and Complementary Non-Destructive Techniques,” *IEEE Trans. Nucl. Sci.*, vol. 61, no. 4, pp. 2137–2143, Aug. 2014, DOI. [10.1109/TNS.2014.2304751](https://doi.org/10.1109/TNS.2014.2304751).
- [9] E. Simon, F. Jallu, B. Pérot, and S. Plumeri, “Feasibility study of fissile mass quantification by photofission delayed gamma rays in radioactive waste packages using MCNPX,” *Nuclear Instrum. and Methods in Phys. Res. A*, vol. 840, pp. 28–35, Dec. 2016, DOI. [10.1016/j.nima.2016.09.047](https://doi.org/10.1016/j.nima.2016.09.047).
- [10] I. Meleshenkovskii, T. Ogawa, A. Sari, F. Carrel, and K. Boudergui, “Optimization of a 9 MeV electron accelerator *Bremsstrahlung* flux for photofission-based assay techniques using PHITS and MCNP6 Monte Carlo codes,” *Nuclear Instrum. and Methods in Phys. Res. B*, vol. 483, pp. 5–14, Nov. 2020, DOI. [10.1016/j.nimb.2020.10.002](https://doi.org/10.1016/j.nimb.2020.10.002).
- [11] M. Delarue, E. Simon, B. Pérot, P. G. Allinei, N. Estre, E. Payan, *et al.*, “Measurement of cumulative photofission yields of  $^{235}\text{U}$  and  $^{238}\text{U}$  with a 16 MeV *Bremsstrahlung* photon beam,” *Nuclear Instrum. and Methods in Phys. Res. A*, vol. 1011, Art. no. 165598, Sep. 2021, DOI. [10.1016/j.nima.2021.165598](https://doi.org/10.1016/j.nima.2021.165598).
- [12] I. Meleshenkovskii, A. Elayeb, R. De Stefano, and A. Sari, “Feasibility study of the photofission technique for radiological characterization of 220-L concrete-lined nuclear waste drums using 7 or 9 MeV linacs,” *Nuclear Instrum. and Methods in Phys. Res. A*, vol. 1029, Art. no. 166422, Apr. 2022, DOI. [10.1016/j.nima.2022.166422](https://doi.org/10.1016/j.nima.2022.166422).
- [13] M. Delarue, E. Simon, B. Pérot, P. G. Allinei, N. Estre, D. Eck, *et al.*, “New measurements of cumulative photofission yields of  $^{239}\text{Pu}$ ,  $^{235}\text{U}$  and  $^{238}\text{U}$  with a 17.5 MeV *Bremsstrahlung* photon beam and progress toward actinide differentiation,” *Nuclear Instrum. and Methods in Phys. Res. A*, vol. 1040, Art. no. 167259, Oct. 2022, DOI. [10.1016/j.nima.2022.167259](https://doi.org/10.1016/j.nima.2022.167259).
- [14] A. Elayeb, A. Sari, I. Meleshenkovskii, R. De Stefano, A. Dabat-Blondeau, and Y. Moline, “Performance Assessment of a New Digital Readout Electronics for Nuclear Waste Drum Characterization by Photofission,” in *2022 IEEE Nuclear Science Symposium and Medical Imaging Conference (NSS/MIC)*, Milan, Italy, Nov. 2022, pp. 1–2, DOI. [10.1109/NSS/MIC44845.2022.10399217](https://doi.org/10.1109/NSS/MIC44845.2022.10399217).
- [15] C. Carasco, D. Eck, B. Geslot, E. Payan, B. Pérot, J. Roullet dit Rouaux, *et al.*, “Photofission delayed gamma-ray measurements in a large cemented radioactive waste drum during linac irradiation,” *Nuclear Instrum. and Methods in Phys. Res. A*, vol. 1053, Art. no. 168360, Aug. 2023, DOI. [10.1016/j.nima.2023.168360](https://doi.org/10.1016/j.nima.2023.168360).
- [16] J. L. Jones, W. Y. Yoon, D. R. Norman, K. J. Haskell, J. M. Zabriskie, S. M. Watson, *et al.*, “Photonuclear-based, nuclear material detection system for cargo containers,” *Nuclear Instrum. and Methods in Phys. Res. B*, vol. 241, no. 1–4, pp. 770–776, Dec. 2005, DOI. [10.1016/j.nimb.2005.07.242](https://doi.org/10.1016/j.nimb.2005.07.242).
- [17] J. L. Jones, D. R. Norman, K. J. Haskell, J. W. Sterbentz, W. Y. Yoon, S. M. Watson, *et al.*, “Detection of shielded nuclear material in a cargo container,” *Nuclear Instrum. and Methods in Phys. Res. A*, vol. 562, no. 2, pp. 1085–1088, Jun. 2006, DOI. [10.1016/j.nima.2006.02.101](https://doi.org/10.1016/j.nima.2006.02.101).
- [18] A. Sari, F. Carrel, A. Grabowski, F. Lainé, B. Espinosa, J. Poli, *et al.*, “Deployment of the First Photofission Measurement System Dedicated to SNM Detection in Europe: Outcomes and Future Prospects,” in *2019 IEEE Nuclear Science Symposium and Medical Imaging Conference (NSS/MIC)*, Manchester, UK, 2019, pp. 1–2, DOI. [10.1109/NSS/MIC42101.2019.9059765](https://doi.org/10.1109/NSS/MIC42101.2019.9059765).
- [19] A. Sari, A. Elayeb, J. Piekar, R. De Stefano, G. Corre, Y. Moline, *et al.*, “Deployment of a 7 MeV Mobile Photofission Inspection System at the Rijeka Seaport for the Detection of SNM in Cargo Containers,” in *2024 IEEE Nuclear Science Symposium (NSS), Medical Imaging Conference (MIC) and Room Temperature Semiconductor Detector Conference (RTSD)*, Tampa, FL, USA, 2024, pp. 1–2, DOI. [10.1109/NSS/MIC/RTSD57108.2024.10655794](https://doi.org/10.1109/NSS/MIC/RTSD57108.2024.10655794).
- [20] A. Sari, A. Elayeb, R. De Stefano, I. Meleshenkovskii, M. Michel, and F. Carrel, “Evaluation of delayed neutron yields and time spectra from photofission of  $^{238}\text{U}$  induced by *Bremsstrahlung* photons below 9 MeV,” in *15th International Conference on Nuclear Data for Science and Technology (ND2022)*, virtual conference, May 2023, Art. No. 11002, DOI. [10.1051/epjconf/202328411002](https://doi.org/10.1051/epjconf/202328411002).
- [21] A. Sari, “Characterization of photoneutron fluxes emitted by electron accelerators in the 4–20 MeV range using Monte Carlo codes: A critical review,” *Appl. Radiat. Isot.*, vol. 191, Art. no. 110506, Jan. 2023, DOI. [10.1016/j.apradiso.2022.110506](https://doi.org/10.1016/j.apradiso.2022.110506).
- [22] Z. Berant, A. Wolf, and R. Moreh, “Detection of fast neutron contamination in photon beams,” *Nuclear Instrum. and Methods*, vol. 140, no. 1, pp. 109–112, Jan. 1977, DOI. [10.1016/0029-554X\(77\)90072-6](https://doi.org/10.1016/0029-554X(77)90072-6).
- [23] A. Wolf, and R. Moreh, “Utilization of teflon-covered Ge(Li) diodes for fast neutron detection,” *Nuclear Instrum. and Methods*, vol. 148, no. 1, pp. 195–197, Jan. 1978, DOI. [10.1016/0029-554X\(78\)90353-1](https://doi.org/10.1016/0029-554X(78)90353-1).
- [24] T. Gozani, J. Stevenson, and M. J. King, “Neutron threshold activation detectors (TAD) for the detection of fissions,” *Nuclear Instrum. and Methods in Phys. Res. A*, vol. 652, no. 1, pp. 334–337, Oct. 2011, DOI. [10.1016/j.nima.2011.01.029](https://doi.org/10.1016/j.nima.2011.01.029).
- [25] M. Hamel, P. Siczynski, P. Blanc, J. Iwanowska, F. Carrel, A. Syntfeld-Kazuch, *et al.*, “A fluorocarbon plastic scintillator for neutron detection: Proof of concept,” *Nuclear Instrum. and Methods in Phys. Res. A*, vol. 768, pp. 26–31, Dec. 2014, DOI. [10.1016/j.nima.2014.09.029](https://doi.org/10.1016/j.nima.2014.09.029).
- [26] P. Siczynski, J. Kownacki, M. Moszyński, J. Iwanowska-Hanke, A. Syntfeld-Kazuch, A. Gójska, *et al.*, “Verification of threshold activation detection (TAD) technique in prompt fission neutron detection using scintillators containing  $^{19}\text{F}$ ,” *Journal of Instrumentation*, vol. 10, Art. no. T09005, Sep. 2015, DOI. [10.1088/1748-0221/2015/09/T09005](https://doi.org/10.1088/1748-0221/2015/09/T09005).
- [27] J. A. Kulesza, T. R. Adams, J. C. Armstrong, S. R. Bolding, F. B. Brown, J. S. Bull, *et al.*, “MCNP® Code Version 6.3.0 Theory & User Manual,” Los Alamos National Laboratory (LANL), Los Alamos, NM, USA, Rep. LA-UR-22-30006, Rev. 1, Sep. 2022, DOI. [10.2172/1889957](https://doi.org/10.2172/1889957).
- [28] M. E. Rising, J. C. Armstrong, S. R. Bolding, F. B. Brown, J. S. Bull, T. P. Burke, *et al.*, “MCNP® Code Version 6.3.0 Release Notes,” Los Alamos National Laboratory (LANL), Los Alamos, NM, USA, Rep. LA-UR-22-33103, Rev. 1, Jan. 2023, DOI. [10.2172/1909545](https://doi.org/10.2172/1909545).
- [29] T. Sato, Y. Iwamoto, S. Hashimoto, T. Ogawa, T. Furuta, S. Abe, *et al.*, “Recent improvements of the particle and heavy ion transport code system – PHITS version 3.33,” *J. Nucl. Sci. Technol.*, vol. 61, no. 1, pp. 127–135, 2024, DOI. [10.1080/00223131.2023.2275736](https://doi.org/10.1080/00223131.2023.2275736).
- [30] Y. Iwamoto, S. Hashimoto, T. Sato, N. Matsuda, S. Kunieda, Y. Çelikb, *et al.*, “Benchmark study of particle and heavy-ion transport code system using shield-ing integral benchmark archive and database for accelerator-shielding experiments,” *J. Nucl. Sci. Technol.*, vol. 59, no. 5, pp. 665–675, 2022, DOI. [10.1080/00223131.2021.1993372](https://doi.org/10.1080/00223131.2021.1993372).